Rain gauge networks' limitations and the implications to hydrological modelling highlighted with a X-band radar

Igor Paz, Ioulia Tchiguirinskaia, Daniel Schertzer

Rain gauge networks' limitations and the implications to hydrological modelling highlighted with a X-band radar

Igor Paz[*1,2], Ioulia Tchiguirinskaia[1] and Daniel Schertzer[1]

[1] HMCO, École des Ponts ParisTech, University of Paris-Est, Champs-sur-Marne 77455, France; ioulia.tchiguirinskaia@enpc.fr (I.T.); daniel.schertzer@enpc.fr (D.S.)

[2] Instituto Militar de Engenharia, Praça General Tibúrcio 80, Rio de Janeiro 22290-270, Brazil

* Correspondence: igor.da-silva-rocha-paz@enpc.fr

Abstract

Precipitation risk and water management is a key challenge for densely populated urban areas. Applications derived from high spatio-temporal resolution observation of precipitations are to make our cities more weather-ready. Finer resolution data available from dual polarised X-band radar measurements enhance engineering tools as used for urban planning policies as well as protection (mitigation/adaptation) strategies to tackle climate-change related weather events. For decades engineering tools have been developed to work conveniently either with very local rain gauge networks, or with mainly C-band radars that have gradually been set up for space-time remote sensing of precipitation. Most of the time, the C-band radars continue to be calibrated by the existing rain gauge networks. Inhomogeneous distributions of these networks lead to only a partial information on the rainfall fields. Here we show that the statistics of measured rainfall is strongly biased by the fractality of the

measuring networks and that this fractality needs to be properly taken into account to retrieve the original properties of the rainfall fields, in spite of the radar data calibration. In this work, we use the semi-distributed hydrological modelling over the Bièvre catchment to generate a virtual rain gauges' network. And, firstly, performing a fractal analysis of this network distribution, we demonstrate that the semi-distributed hydrological models statistically reduce the distributed (weather radar) rainfall fields into rainfall measured by a much scarcer network of virtual rain gauges. Then, with the help of the Intersection Theorem and multifractal theory, we statistically compare the virtual rain gauges' data with the rainfall data measured by the dual-polarimetric X-band radar operated at Ecole des Ponts with a spatial resolution of 250 m, providing pre-factors that indicate the need of a proper re-normalisation of rain gauge rainfall data when comparing (or calibrating) with radar data and the possible counterproductivity of this conditioning.

Keywords: rain gauge network; spatio-temporal variability; X-band radar; fractals; multifractals; semi-distributed hydrological model

1. Introduction

The increase in global urbanisation and population density emphasises the importance and the need to improve the adaptation of urban areas mainly to climate change (Pumo et al., 2017; Arnone et al., 2018). Managing extreme weather events, particularly intense precipitation ones and heat waves, in these areas is a major challenge for the future. The population's demand for a better quality of life motivates an improvement in the ability to measure, understand,

model and predict hydrometeorological processes in urban environments, aiming at better flood control and associated risk management. Conventional local measurements in urban areas generally do not meet the World Meteorological Organization (WMO) criteria for the measurement of precipitation (WMO, 2014). Better spatio-temporal scales with accuracy and reliability are required (Fabry et al., 1994; Berne et al., 2004). In this way, the use of ground-based remote sensing has been very important in elucidating complex urban environment structures, thus expanding hydrometeorological challenges (NRC, 2012).

Weather radars have the capability to estimate rainfall fields with high spatio-temporal resolutions and have been used to cope the sparseness of rain gauge networks. Nevertheless, the initial measurement of reflectivities adopted by those devices, not providing direct precipitation rates such as rain gauges, usually generates significant uncertainties. Then, with the growing use of radars to estimate rain rates, many studies have been developed to adjust and/or merge weather radars (mostly considering non-polarimetric ones) with rain gauge networks (Einfalt et al., 2005; Allegretti et al., 2012; Lo Conti et al., 2015). On the other hand, especially for high rainfall intensities, in order to reduce these uncertainties and improve the rainfall estimates, dual polarisation technology using specific differential phase (KDP) has been employed, which does not necessarily requires rain gauge adjustments according to some authors (Bringi and Chandrasekar 2001; Illingworth and Blackman 2002; Figueras i Ventura et al., 2012; Chandressekar et al., 2015). This technology explores the flatness of large raindrops to analyse the phase difference of the

reflected vertical and horizontal signals and then directly obtain the precipitation rates.

Coming together with rainfall data improvement, an efficient storm water management also deals with the accuracy and reliability of hydrological models, mainly in urban areas which present higher levels of imperviousness leading to shorter response times (Berne et al., 2004; Segond et al., 2007; Furusho et al., 2014; Ochoa-Rodriguez et al., 2015; Arnone et al., 2018). This requests the use of high resolution models, which means reducing the size of the sub-catchments in the semi-distributed models or adopting the fully-distributed models (Fewtrell et al., 2011; Ichiba, 2016; Pina et al., 2016; Pumo et al., 2017; Alves de Souza et al., 2018; Paz et al., 2019).

This work presents a discussion of the rain gauge networks' limitations and the implications to hydrological modelling with the help of fractal and multifractal analysis. The study was carried out over the Bièvre catchment, which is a 110 km^2 semi-urbanised area located in the southwest of Paris region, using the rainfall data of the dual-polarimetric X-band radar recently installed on the roof of the École des Ponts ParisTech (ENPC).

The paper is organised in five sections. Section 2 describes the case study and the rainfall data. The methodology of fractal and multifractal analyses are presented in Section 3. Section 4 presents the results and discussion. And finally, the conclusions are presented in Section 5.

2. Case Study and Rainfall Data

The Bièvre Valley, which is a 110 km2 semi-urbanised area in the southwest of Paris region, was selected as case study. The Bièvre River is 33

km-long tributary of the Seine River and its upstream catchment is managed by two local authorities: the CASQY ("Communauté d'Agglomération de Saint-Quentin-en-Yvelines" – Saint-Quentin-en-Yvelines Agglomération Community) in the upstream portion and the SIAVB ("Syndicat Intercommunal d'Assainissement de la Vallée de la Bièvre" – Inter-municipal local authority for Sanitation of the Bièvre Valley) in the downstream portion.

The Bièvre catchment was modelled using InfoWorks CS (Collection Systems) (Paz, 2018; Paz et al., 2018), a widely used semi-distributed model (Soft, 2010), with the operation responsibility given to the company Veolia since 1991 by the local authority SIAVB to perform a real time control of the hydrological area. This hydrological model is integrated in the Optim Sim platform, developed by Veolia, that mimics the actual regulation of the storage basins (Paz, 2018; Paz et al., 2018) in two simulation modes: the "replay mode" and the "forecasting mode". The first one extracts rainfall data from the 6 SIAVB rain gauges' network database (using the Thiessen polygons technique) to replay past events. And the "forecasting mode" uses different rainfall data, e.g. from weather radar measurements, to simulate the catchment hydrological behaviour. The catchment area is divided into 27 sub-catchments, as displayed on Figure 1.

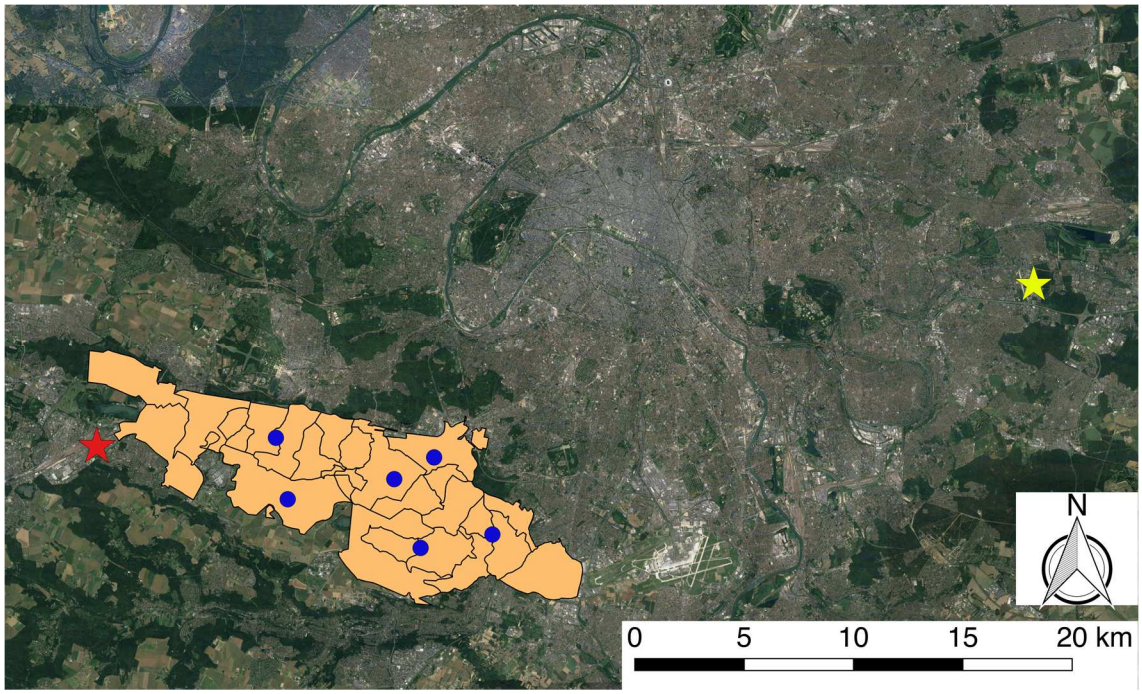

120

121 *Figure 1: Illustration of rainfall measurement devices available over the Bièvre catchment: the X-band radar (yellow*

122 *star), the C-band radar (red star) and the six rain gauges (blue dots).*

123 This modelling had been firstly calibrated using the rainfall data from the
124 Météo-France C-band radar of Trappes, located in a direct proximity (~ 0 - 20
125 km) of the catchment (see Fig. 1), with a resolution of 1 km x 1 km x 5 min.
126 These C-band radar data are firstly obtained as reflectivity (dBZ) and then, after
127 some post-treatments and filtering process, they are transformed into rainfall
128 intensity (R) by applying the Marshall-Palmer Z-R equation (Marshall and
129 Palmer, 1948), with fixed parameters $a = 200$ and $b = 1.6$ (Eq. (1)), which
130 means that the polarimetric capability of this radar of Trappes has not been
131 used. In addition, this catchment also contains a network of six tipping bucket
132 rain gauges (see Fig. 1), which had been used to calibrate the C-band radar
133 data.

$$Z = aR^b \quad (1)$$

134

However, in this study, we used rainfall data from the ENPC dual-polarimetric X-band radar of Champs-sur-Marne (see Fig. 1), with distances ranging between 25 to 45 km and a 250 m x 250 m x 3.41 min resolution. The ENPC X-band Dual Polarization Surface Rainfall Intensity (DPSRI) product still considers the Z-R relationship for low intensities, but for high intensities it uses the specific differential phase (KDP) (Selex, 2015):

$$R = 19.63|KDP|^{0.823}, \quad for\ Z > 35\ dBZ\ and\ KDP > 0.3^{o}/km \tag{2}$$

For the purpose of this work, six different rainfall events were selected: 12-13/09/2015 (44 hours); 16/09/2015 (11.3 hours); 05-06/10/2015 (31 hours); 21-23/05/2016 (59.5 hours); 28-31/05/2016 (87.7 hours); and 17/06/2016 (24 hours).

3. Methods: (multi)fractals

When studying some objects of very irregular or fragmented form (with unusual properties in classical geometry), Mandelbrot (1974) named them as "fractals" ("fractus" means irregular in Latin). Nevertheless, fractal objects must not just be irregular, but also scale invariant, which means that their form remains unchanged at different scales of observation. This brings the properties of self-similarity (a zoomed part of the object looks similar to the object itself, with an isotropic variation) and self-affinity (when the variation is anisotropic).

In classical geometry, dimensions are integers characterising regular spaces as straight lines (1D), planar figures (2D) and volumes (3D). If we take an object, embedded in an Euclidian dimension D, of linear size L, it can be covered by N small objects of linear size l, with a scale ratio λ ($= L/l$).

In the case of fractal objects and sets, the dimension is no longer an integer and is called fractal dimension (D_f) (Mandelbrot, 1967, 1977; Mandelbrot and Pignoni, 1983; Feder, 1988). Even if its theoretical computation is rather complex, an easier way to evaluate it is through the box-counting method (Hentschel and Procaccia, 1983; Lovejoy et al., 1987). It takes into account that when $\lambda \rightarrow \infty$ there is a power-law relation between the fractal dimension and the number of "non-empty" pixels of the set (N_λ) at the scale λ:

$$N_\lambda \approx \lambda^{D_f} \tag{3}$$

where ≈ means the asymptotic equivalence.

Therefore, the box-counting method can be easily applied considering a simple methodology to change the resolution of a given dataset. Let us define A as the geometrical set (embedded in a space of dimension D; in this paper we will consider the 2-D space) to be analysed and $N_{\lambda,A}$ the number of non-overlapping pixels at the resolution λ necessary to cover the set A. Thus, the method consists in firstly counting the number of non-empty pixels at the smallest pixel size (l), then we multiply the pixel size by two at each step of process (practically, it means that in the 2-D case we merge 4 by 4 pixels at each scale variation step) and count again the number of non-empty pixels at this new size, and we continue this procedure until we achieve the maximum pixel size (L). Once we have counted the numbers of non-empty pixels (N_λ) at different scales (λ), we display them in a log-log plot ($\lambda \; vs \; N_\lambda$). Then, if A is a fractal set, the points of this plot will be along a straight line, and, from Eq. (1), we can estimate the fractal dimension D_f as its slope.

Furthermore, the codimension of a fractal set is usually (geometrically) defined as (Mandelbrot, 1967, 1977; Feder, 1988; Falconer, 1990):

$$c = D - D_f \tag{4}$$

Then, it is also possible to probabilistically define the fractal codimension, using Eqs. (3) and (4), where the probability that a cube embedded in the set $\mathbb{R}^D$ at a scale λ is contained in the fractal set is given by:

$$\lambda^{D-D_f} \approx \lambda^c \tag{5}$$

This last definition is more general because it enables $c > D$, which would imply $D_f < 0$ from Eq. (4).

The concept of fractal dimension is related to the sparseness of a dataset and it is well applied to binary fields (e.g., rainfall occurrence, rain gauge network distribution). Many geophysical fields with different intensity levels, and also irregular geometries and scale invariance, can be seen as fractal fields at different thresholds (singularities). Then, for each singularity it is possible to calculate its fractal dimension, which means that the field is characterised by several fractal dimensions according to the imposed threshold (Grassberger, 1983; Hentschel and Procaccia, 1983; Schertzer and Lovejoy, 1984); i.e., for each given threshold, a different fractal dimension is estimated for the field that exceeds the threshold. These fields were named by Parisi and Frisch (1985) as “multifractals”.

Multifractals rely on the assumption that a geophysical field is generated through a multiplicative cascade process (Schertzer and Lovejoy, 1987, 2011)

produced by random multiplicative modulation of large-scale structures into small-scale ones. Furthermore, rainfall fields have been widely studied as presenting multifractal behaviour (Schertzer and Lovejoy, 1987; Ladoy et al., 1993; Tessier et al., 1993; Olsson et al., 1996; de Lima et al., 1999; Deidda, 2000; Veneziano et al., 2006; García-Marin et al., 2008; Serinaldi, 2010; Ochoa-Rodriguez et al., 2015; Paz, 2018).

As just mentioned, the multifractal fields are characterised by a hierarchy of fractal dimensions (and codimensions). Then, by referring to the notion of fractal codimension, one can calculate, for a given multifractal field ε_λ, the probability of obtaining a singularity of order greater than or equal to γ at the scale λ:

$$\Pr(\varepsilon_\lambda \geq \lambda^\gamma) = \frac{\lambda^{D_f(\gamma)}}{\lambda^D} \approx \lambda^{-c(\gamma)} \quad 6)$$

where the codimension function $c(\gamma) = D - D_f(\gamma)$ is convex and increases with λ.

Additionally, multifractal fields can also be described by their statistical moments. Schertzer and Lovejoy (1987, 1991) introduced the scaling moment function $K(q)$, which is also convex and characterises the various q^{th} order statistical moments of the multifractal field ε_λ:

$$\langle \varepsilon_\lambda^q \rangle \approx \lambda^{K(q)} \quad 7)$$

where q is the statistical moments order and $\langle \varepsilon_\lambda^q \rangle$ is the q^{th} moment mean of the intensities at the scale λ.

Furthermore, Parisi and Frisch (1985) demonstrated that the two functions $c(\gamma)$ and $K(q)$ have a one-to-one relationship, which is highlighted by the Legendre transform:

$$K(q) = max_{\gamma}\{q\gamma - c(\gamma)\} \Leftrightarrow c(\gamma) = max_{q}\{q\gamma - K(q)\} \quad (8)$$

These related expressions bring the correspondence between the orders of moments (q) and the singularities (γ), such that:

$$q_{\gamma} = c'(\gamma)\ ;\ c(\gamma) = q_{\gamma}\gamma - K(q_{\gamma}) \quad (9)$$

$$\gamma_{q} = K'(q)\ ;\ K(q) = q\gamma_{q} - c(\gamma_{q}) \quad (10)$$

where at the moment of order q corresponds the singularity γ_q, and conversely, at the singularity γ corresponds the order of moment q_{γ}. In addition, it is possible to see from Eq. (6) that more rare rainfall events (with very large singularities γ) correspond to bigger values of $c(\gamma)$. Consequently, due to the convexity of both $c(\gamma)$ and $K(q)$ and to the Legendre transform, for $q > 1$, these extreme events also correspond to bigger values of q and $K(q)$.

As both statistical functions $c(\gamma)$ and $K(q)$ have the only constraint of convexity, there is an infinity of parameters required to characterise a multifractal process. However, Schertzer and Lovejoy (1987, 1997) explored the concept of universality (usually used in physics, where among an infinite number of parameters only a few would be relevant) and developed the Universal Multifractals (UM) (see Schertzer and Lovejoy, 2011, for a more recent review). In this context, $c(\gamma)$ and $K(q)$ can be fully described by only three "UM parameters" (α, C_1 and H) as:

$$\mathrm{K(q)} = qH + \begin{cases} \frac{C_1}{\alpha - 1}(q^\alpha - q) \; ; \; \alpha \neq 1 \\ C_1 \, q \log(q) \quad ; \; \alpha = 1 \end{cases} \quad (1$$

$$\mathrm{c}(\gamma + H) = \begin{cases} C_1 \left(\frac{\gamma}{C_1 \alpha'} + \frac{1}{\alpha} \right)^{\alpha'} \quad ; \; \alpha \neq 1 \\ C_1 \, exp\left(\frac{\gamma}{C_1} - 1 \right) \quad ; \; \alpha = 1 \end{cases} \quad (1$$

245

246 where $\frac{1}{\alpha} + \frac{1}{\alpha'} = 1$, for all $\alpha \neq 1$, and:

247 – α is the Levy's multifractality index ($0 \leq \alpha \leq 2$). It measures the degree of
248 multifractality of the process. In particular, if $\alpha = 0$ we observe a monofractal
249 process (also entitled β-model, Mandelbrot (1974)) and $\alpha = 2$ corresponds to
250 the maximum of multifractality for a model (improperly called lognormal);
251 – C_1 is the codimension of the mean singularity of the field. It measures the
252 mean inhomogeneity, where $C_1 = 0$ for a homogeneous field. The more it
253 increases, the more the singularity of the field average is dispersed. We thus
254 observe a field rarely exceeding its mean, but which can do so in an
255 extremely strong way;
256 – H is the Hurst's exponent, which measures the degree of non-conservation of
257 the field. Values of H close to zero indicate higher conservativeness of the
258 process.

259

260 While performing a multifractal analysis of a (rainfall) field, we should
261 determine its statistical functions $c(\gamma)$ and $K(q)$. The Trace Moment (TM)
262 method (Schertzer and Lovejoy, 1987) allows to directly determine the scaling
263 moments function $K(q)$ for any $q > 0$.

As $K(q) > 0$ for $q > 1$, $\langle \varepsilon_\lambda^q \rangle \approx \lambda^{K(q)} \to \infty$ when $\lambda \to \infty$. Then, to avoid this divergence, the concept of flux (Π_λ) is used, given by:

$$\Pi_\lambda = \int \varepsilon_\lambda \, d^D x \tag{13}$$

And the trace of the q^{th}-power of the flux is:

$$Tr\left[\varepsilon_\lambda^q\right] = \left\langle \int (\varepsilon_\lambda)^q \, d^{qD} x \right\rangle \approx \lambda^{K(q)-D(q-1)} \tag{14}$$

In practice, the method consists in taking the q^{th}-power of each value of the field ε_λ at the scale λ, and then the ensemble average of q^{th}-power moments is calculated at that scale. Then, from Eq. (14), the same process is repeated for different scales λ, the resulting averages are displayed as a function of λ in a log-log plot, and a linear regression is performed to obtain the value of $K(q)$ (which will be estimated as the given slope). Finally, by repeating this process also with other values of q, we obtain the $K(q)$ function (and, via Legendre transform, the $c(\gamma)$ function).

Thus, once we know $K(q)$, it is possible to (indirectly) determine the UM parameters α and C_1:

$$C_1 = K'(1) \tag{15}$$

$$\alpha = K''(1)/C_1 \tag{16}$$

In the framework of UM, Lavallée et al. (1993) developed the Double Trace Moment (DTM) method to directly determine the parameters α and C_1, which means that there is no need to firstly obtain $K(q)$ (and $c(\gamma)$). This

technique is in fact a generalisation of the TM method and considers that the q^{th}-order moments of the renormalised η-power of a conservative field ε_λ remain scale invariant. Then, the idea is to apply the TM method to this renormalised field (through the $K(q,\eta)$ function):

$$\langle\left(\varepsilon_\lambda^{(\eta)}\right)^q\rangle \approx \lambda^{K(q,\eta)} \Rightarrow \langle\frac{\varepsilon_\lambda^{\eta q}}{\langle\varepsilon_\lambda^{\eta}\rangle^q}\rangle \approx \frac{\lambda^{K(q\eta)}}{\lambda^{qK(\eta)}} = \lambda^{K(q\eta)-qK(\eta)} \quad (17)$$

where $\varepsilon_\lambda^{(\eta)} = \frac{\varepsilon_\lambda^{\eta}}{\langle\varepsilon_\lambda^{\eta}\rangle}$.

Then:

$$K(q,\eta) = K(q\eta) - qK(\eta) \quad (18)$$

Since this method is especially applied for UM, considering Eq. (11), Eq. (18) becomes:

$$K(q,\eta) = \eta^\alpha K(q) \quad (19)$$

From Eq. (19), the parameter α can be directly estimated as the slope of the linear part of $K(q,\eta)$ vs. η in a log-log plot, for a given q. And in the same log-log plot, the parameter C_1 can be also estimated from the interception value of the linear part and the axis $\log(\eta) = 0$ (Hoang, 2011).

In addition, according to the Intersection Theorem (Schertzer and Lovejoy, 1987), considering two independent (multi)fractal fields $\varepsilon_{1,\lambda}$ and $\varepsilon_{2,\lambda}$ embedded in the same space and presuming that the intersection of both ($\varepsilon_{1,\lambda} \cap \varepsilon_{2,\lambda}$) is not empty, for the given intersection the probability of obtaining a singularity of order greater than or equal to γ at the scale λ is:

$$\Pr\left(\varepsilon_{1,\lambda} \cap \varepsilon_{2,\lambda} \geq \lambda^{\gamma}\right) = \Pr\left(\varepsilon_{1,\lambda} \geq \lambda^{\gamma}\right) \Pr\left(\varepsilon_{2,\lambda} \geq \lambda^{\gamma}\right) \quad 20)$$

Therefore, following Eq. (6), the resulting codimension is the addition of independent (multi)fractal processes:

$$c_{\varepsilon_1 \cap \varepsilon_2}(\gamma) = c_{\varepsilon_1}(\gamma) + c_{\varepsilon_2}(\gamma) \quad 21)$$

In the following Section, we will use the fractal and multifractal (with the help of the DTM method and the Intersection Theorem) approaches to discuss the rain gauge networks' limitations and the implications to hydrological modelling.

4. Results and Discussion

In this work, the sub-catchments' distribution of the pilot site of Bièvre catchment, which had already been modelled with the semi-distributed model InfoWorks CS (Paz, 2018; Paz et al., 2018), was used to construct a network of virtual rain gauges located in the centre of mass of each sub-catchment. Then, an area of 8 km x 8 km was selected using the X-band radar grid (Fig. 2). This choice corresponds to the most homogeneous distribution of virtual rain gauges over a square area of Bièvre catchment, containing 15 of the 27 virtual rain gauges.

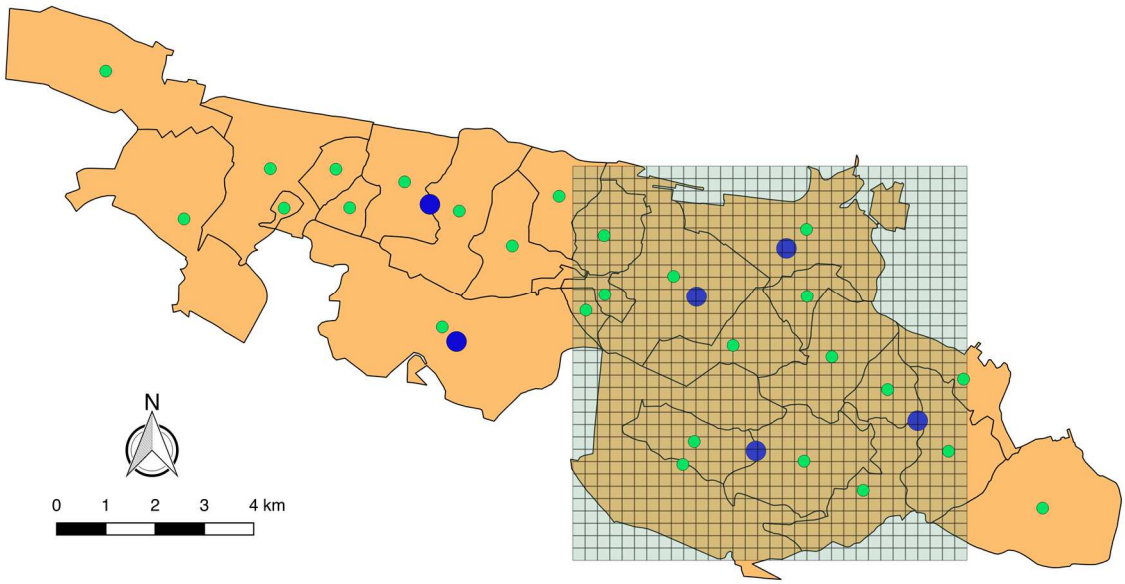

Figure 2: Virtual rain gauges' distribution (green dots) and 6 SIAVB rain gauges (blue dots) over the 27 sub-catchments, and the 8 km x 8 km selected ENPC X-band radar grid.

Four different rainfall fields have been analysed over the selected area (Fig. 3): (a) original radar data; (b) original radar data corresponding to each centroid pixel; (c) sub-catchment averaged rainfall radar data; (d) sub-catchment averaged rainfall radar data being concentrated at the corresponding centroid pixel; as well as a (e) fractal distribution of the corresponding virtual rain gauges, located at the centroid pixels.

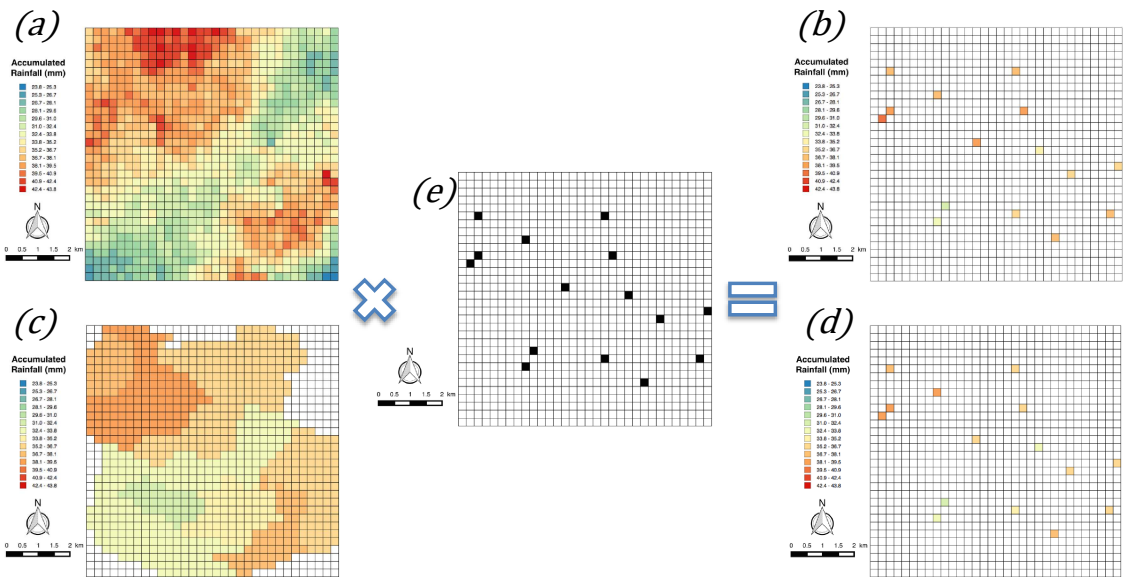

Figure 3: Four different rainfall radar data fields analysed over the selected area (demonstrated here with data of the 12 September 2015 event): (a) original data; (b) original data corresponding to each centroid pixel; (c) sub-catchment averaged rainfall; (d) sub-catchment averaged rainfall being concentrated at the corresponding centroid pixels. And the 15 sub-catchment centroid pixels corresponding to the virtual rain gauges' locations (e).

Firstly, the fractal analysis of the 15 virtual rain gauge pixels' distribution (which will also be called rainfall support) was performed using the box-counting method (Fig. 4) with a simple Scilab routine (Gires et al., 2017, 2018), which applies the methodology described in the previous section (see Eq. (3)) to the dataset. It is possible to identify a scaling break (with two different behaviours for the small scales and the large scales) at the spatial scale of 2 km, which is in fact the average sub-catchment's size and close to the 1-km resolution of the C-band radar rainfall data that have been used for the model calibration. Then, a relatively high fractal dimension (D_f = 1.66) obtained over the large-scale range

corresponds to the network of 15 virtual rain gauges at 2-km scale. This number of gauges remains still reasonable, although only 6 real rain gauges are available for the full Bièvre catchment (i.e. 4 over the selected area). Preserving the same fractal dimension D_f = 1.66 over smaller scales up to 250 m (the resolution of the X-band radar rainfall) would result in N = 315 virtual rain gauges (and/or sub-catchments). Thus, a smaller number of gauges (N = 15), characterised by much lower fractal dimension (D_f = 0.185), significantly reduces the captivity of spatial rainfall variability over small scales and hence its representability in the model having a constant rainfall per sub-catchment of 2-km characteristic scale.

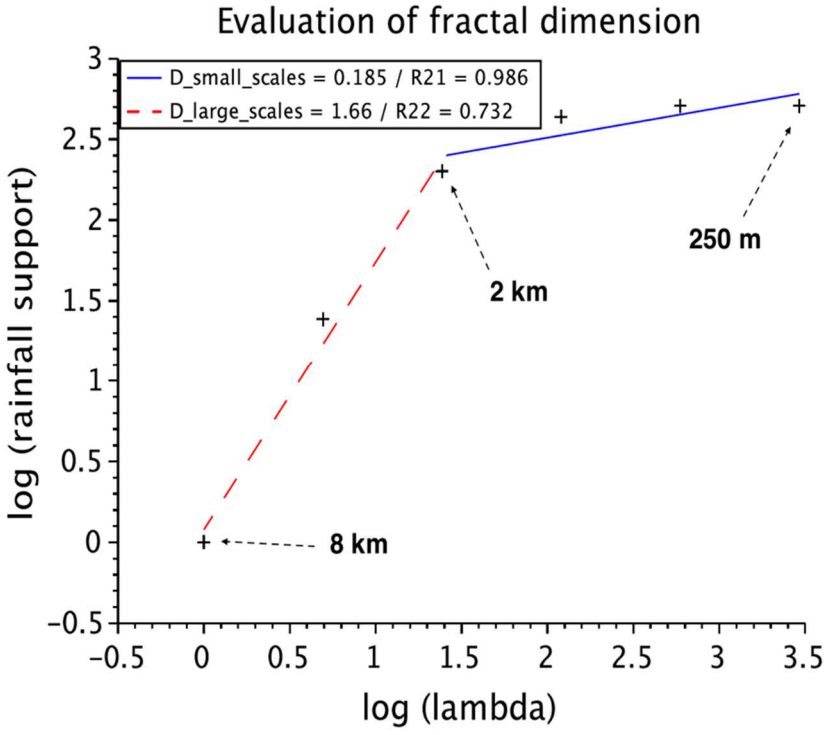

Figure 4: Fractal analysis of the centroid pixels' distribution, providing the linear regression coefficients R21 (small scales) and R22 (large scales).

This result from the fractal analysis of the 15 virtual rain gauge network distribution corroborates the researches from Austin (1987), Schertzer and Lovejoy (1987), Seed and Austin (1990), Vieux and Vieux (2005), Villarini et al.

(2008), Peleg et al. (2013), which identify the difficulties of sparsely distributed rain gauge networks to capture the high spatial and temporal variability of precipitation fields (specially high convective ones), while comparing to weather radars. On the other hand, when dealing with the sub-catchment sizes, it also confirms the findings of Thorndahl et al. (2017), based on a review of the state of the art about the use of weather radar rainfall data in urban hydrology (Schilling, 1991; Berne et al., 2004; Einfalt et al., 2004; Ochoa-Rodriguez et al., 2015), in which they associate the better spatial and temporal resolution of radar rainfall data to decreasing catchment sizes.

Then, to better evaluate the unfortunate consequences of sparse rain gauge networks, the multifractal analyses were performed over the studied rainfall fields in conditions (a), (b), (c) and (d), and then related to the fractal analysis of the rain gauge's distribution with the help of the Legendre transform. Firstly, the DTM method was applied (Fig. 5), following the methodology described in Section 3 (Eq. (19)), on ensemble of data over the whole rainfall event (each time step being considered as an independent realisation) with scaling break. The values obtained for α and C_1 for the six studied events are presented at Tables: 1 (rainfall fields (a)), 2 (rainfall fields (b)), 3 (rainfall fields (c)) and 4 (rainfall fields (d)).

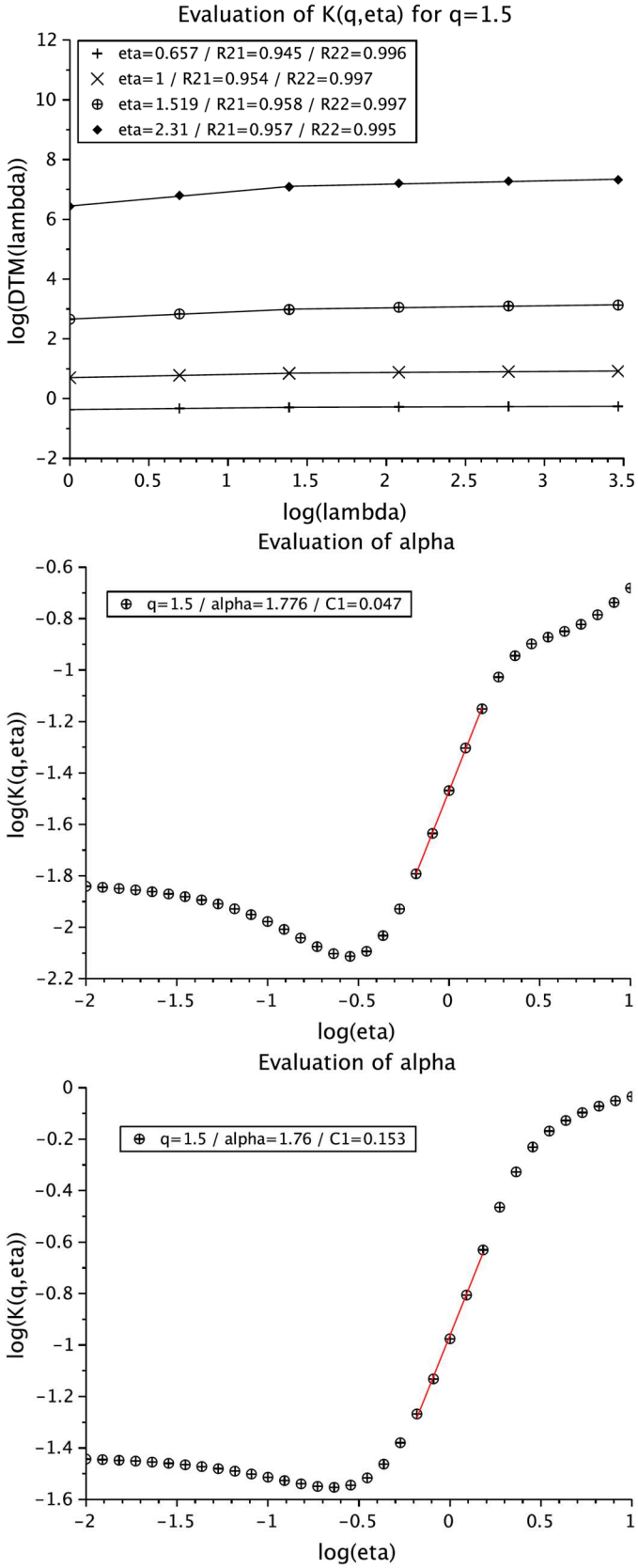

Figure 5: Application of DTM method (demonstrated here with data of the 12-13 September 2015 event): Evaluation of empirical $K(q,\eta)$ with scaling break at 2 km,

providing the linear regression coefficients R21 (small scales) and R22 (large scales) (top); Evaluation of α at small scales (centre); Evaluation of α at large scales (bottom).

Events	Small Scales		Large Scales	
	α	C_1	α	C_1
12-13/09/2015	1.776	0.047	1.76	0.153
16/09/2015	1.676	0.027	0.922	0.094
05-06/10/2015	2.029	0.05	1.775	0.189
21-23/05/2016	1.324	0.041	1.242	0.161
28-31/05/2016	1.656	0.045	1.665	0.199
17/06/2016	1.305	0.127	1.058	0.574

Table 1: Estimated UM parameters for rainfall fields in condition (a).

Events	Small Scales		Large Scales	
	α	C_1	α	C_1
12-13/09/2015	-0.009	1.757	0.746	0.659
16/09/2015	0.023	1.769	0.244	0.539
05-06/10/2015	0.07	1.788	0.636	0.623
21-23/05/2016	0.015	1.778	0.295	0.571
28-31/05/2016	-0.003	1.761	0.613	0.64
17/06/2016	-0.009	1.753	0.487	1.016

Table 2: Estimated UM parameters for rainfall fields in condition (b).

Events	Small Scales		Large Scales	
	α	C_1	α	C_1
12-13/09/2015	0.642	0.087	1.397	0.131

16/09/2015	0.247	0.075	0.602	0.092
05-06/10/2015	0.684	0.09	1.421	0.152
21-23/05/2016	0.309	0.083	0.844	0.127
28-31/05/2016	0.493	0.084	1.31	0.149
17/06/2016	0.661	0.123	0.969	0.341

396 *Table 3: Estimated UM parameters for rainfall fields in condition (c).*

397

Events	**Small Scales**		**Large Scales**	
	α	C_1	α	C_1
12-13/09/2015	-0.014	1.751	0.66	0.6
16/09/2015	0.011	1.762	0.153	0.514
05-06/10/2015	0.039	1.769	0.515	0.591
21-23/05/2016	-0.003	1.763	0.278	0.545
28-31/05/2016	-0.019	1.75	0.587	0.601
17/06/2016	-0.006	1.749	0.545	0.871

398 *Table 4: Estimated UM parameters for rainfall fields in condition (d).*

399

400 Due to the fact that the rainfall fields (condition (a)) and the virtual rain
401 gauge's network distribution (condition (e)) are fully independent, the
402 Intersection theorem (see Section 3) implies that the codimension function of
403 their product (condition (b)) will correspond to the following sum of the
404 codimension functions:

$$\mathrm{c}_{(b)=(a)\cap(e)}(\gamma) = \mathrm{c}_{(a)}(\gamma) + \mathrm{c}_{(e)}(\gamma) \quad (22)$$

405

406 And then, by Legendre transform (see Section 3), the scaling moment
407 function of the product (condition (b)) will correspond to the sum of the scaling

408 moment functions of the rainfall field (condition (a)) and the virtual rain gauge
409 network (condition (e)):

$$\mathrm{K}_{(b)=(a)\cap(e)}(q) = \mathrm{K}_{(a)}(q) + \mathrm{K}_{(e)}(q) \quad (23)$$

410

411 The relationships similar to Eqs. (22) and (23) stand for the rainfall fields
412 (condition (c)), virtual rain gauge network (condition (e)) and their product
413 (condition (d)) as well. Figures 6 and 7 present the theoretical $K(q)$ curves for
414 all fields taking into account the estimated values (from Fig. 4 and Tables 1, 2, 3
415 and 4), for small scales (250 m – 2 km) and large scales (2 km - 8 km)
416 respectively; considering that α was simulated as 0 when the estimated $\alpha < 0$,
417 and as 2 when the estimated $\alpha > 2$.

418

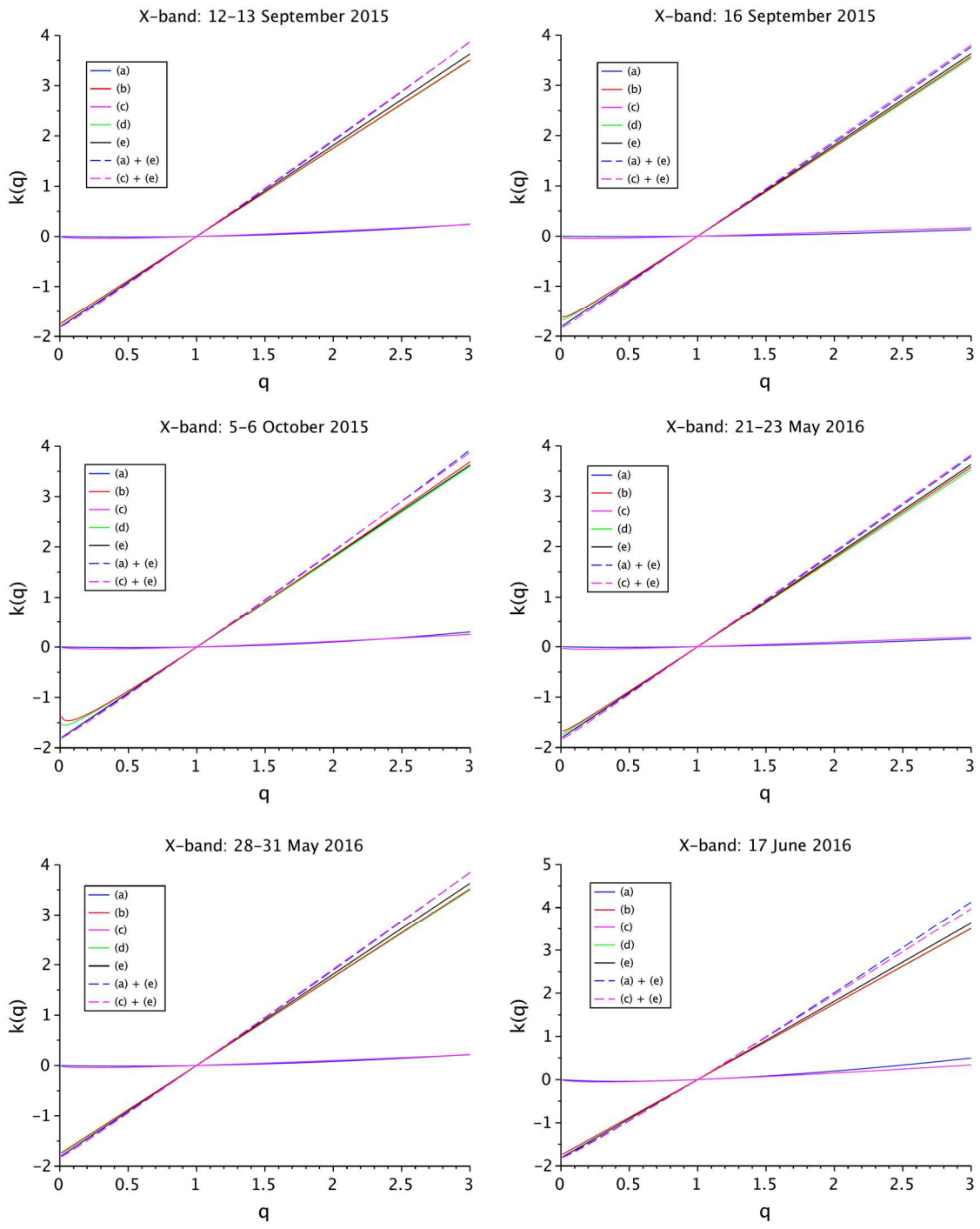

Figure 6: $K(q)$ relations at small scales for the six studied events.

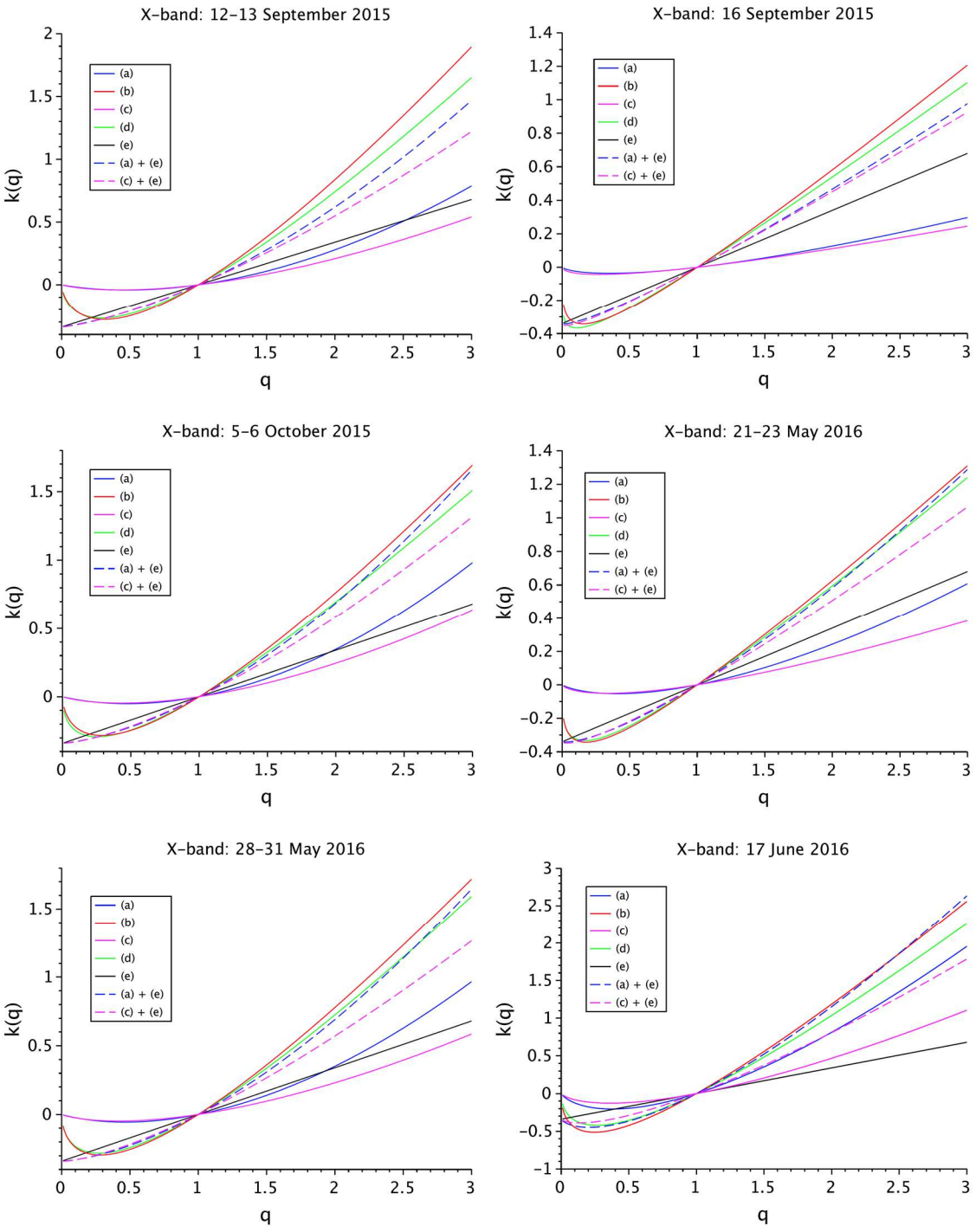

Figure 7: $K(q)$ relations at large scales for the six studied events.

From Figure 6 one may note that the monofractality of fields (b) and (d) at small scales (denoted by the estimated α values close to 0 in Tables 2 and 4, respectively) affects the suitability of the Intersection Theorem (see Section 3

and Eq. (23)). On the other hand, for the large scales in Figure 7 the theoretical expression given by Eq. (23) works better for some of the events than for others: the $\mathrm{K}_{(a)}(q) + \mathrm{K}_{(e)}(q)$ curves fit better the $\mathrm{K}_{(b)}(q)$ ones for 05-06/10/2015, 21-23/05/2016, 28-31/05/2016 and 17/06/2016 events than those for 12-13/09/2015 and 16/09/2015 events. This could be easily understood by evaluating the linear term of the Eq. (23). Indeed, the scaling moment function of the network will correspond to the β-model, using Eq. (4):

$$\mathrm{K}_{(e)}(q) = c(q-1) \tag{24}$$

where over the large scales: $c = 2 - 1.66 = 0.34$, and this is independently either of rainfall events, or rainfall fields.

Then:

$$\mathrm{K}_{(b)}(q) = \frac{C_1}{\alpha - 1}(q^\alpha - q) + c(q-1) = \frac{C_1}{\alpha - 1}q^\alpha - \left(\frac{C_1}{\alpha - 1} - c\right)q - c \tag{25}$$

The resulting scaling moment function is no longer UM function, but still could be well approximated by it, at least between statistical moments of the orders 1-3, when the pre-factor $\left(\frac{C_1}{\alpha-1} - c\right)$ of the linear term remains positive. With $c = 0.34$ and UM parameters from Tables 1 and 3 over large scales one may obtain the following estimates (Tab. 5) of these pre-factors for conditions (a) and (c):

Events	Rainfall field (a)	Rainfall field (c)

12-13/09/2015	-0.139	-0.01
16/09/2015	-1.545	-0.571
05-06/10/2015	-0.096	0.021
21-23/05/2016	0.325	-1.154
28-31/05/2016	-0.041	0.141
17/06/2016	9.557	-11.34

Table 5: Estimated pre-factors over large scales for rainfall fields in conditions (a) and (c).

Finally, the results from the multifractal analyses presented in this section indicate a twofold discussion: (i) the events with stronger negative values of the pre-factor give less empirical agreement with the theoretical expression of Eq. (23); (ii) and, on the contrary, a larger positive pre-factor leads to a much stronger convergence between the theoretical and empirical curves.

5. Conclusions

In this study we performed (multi)fractal analysis on rain gauge network and X-band radar rainfall data in the context of (urban) hydrological modelling. The main objectives of this work are to analyse the impacts of the rainfall data spatio-temporal variability on hydrological modelling, presenting the limitations of sparse rain gauge networks compared to high-resolution radar data, and to discuss the suitability of radar-rain gauge conditioning considering the fractality of rain gauge networks.

This paper takes the the Bièvre catchment, which is a semi-urbanised area of 110 km^2 located in the southwest of Paris region, as a case study. In this work, we used the semi-distributed modelling distribution of this area performed with the InfoWorks CS and considered a virtual rain gauge in the centre of mass of each sub-catchment. Then, we compared the rainfall data

distributions of the virtual rain gauge network with those obtained from the ENPC dual-polarised X-band radar. Firstly, we performed a fractal analysis of the virtual rain gauge network distribution and identified a scaling break at 2 km. Then we took advantage of the Intersection Theorem associated to the multifractal theory to analyse the relationship between both rain gauge and radar data.

The obtained results suggest that the semi-distributed hydrological models statistically reduce the rainfall fields into rainfall measured by a much scarcer network of virtual rain gauges and that inhomogeneous distributions of rain gauging networks lead to only partial information on the rainfall fields. A scaling break is retrieved in the fractal analysis of the virtual rain gauge distribution at the scale of 2 km, which is close to the average sub-catchment's size. The fractality of the rainfall support (here represented by the fixed number of 15 virtual rain gauges over the selected 8 km x 8 km area) is biased by this distribution, where the small-scale behaviour is clearly different of the large-scale one. This implies that, to respect the rainfall support fractality and its capability to consider the rainfall variability over the small scales, the same fractality of the large scales should be found at the small scales. In fact, the statistics of measured rainfall are strongly biased by the fractality of the measuring networks. This fractality needs to be properly taken into account to retrieve the original properties of the rainfall fields, in spite of the radar data calibration.

Additionally, a proper rainfall data re-normalisation is needed when comparing gauged rainfall with the radar data, and consequently when quantifying the impacts of space-time variability within hydrological modelling.

One may also note that a conditioning by the rain gauges could be rather counterproductive for rainfall events with $\frac{C_1}{\alpha-1}$ being weaker than the codimension of the fractal rain gauge networks.

Furthermore, since the Bièvre catchment was calibrated to C-band radar data, in case of the number and distribution of the virtual rain gauges would be reliable in comparison to the C-band radar resolution (1 km^2) – actually the SIAVB network has only 6 rain gauges –, the number of rain gauges to perform the calibration of better-resolution radar data (e.g. non polarimetric X-band radar) should be big enough to respect the same fractality of the big scales. This also means that the size of the sub-catchments should be comparable to the resolution of the rainfall data used, which would drastically increase the number of sub-catchments and become unmanageable.

Funding: This research was partially funded by the Chair "Hydrology for Resilient Cities" endowed by Veolia, and by the Department of Science and Technology of the Brazilian Army.

Acknowledgments: The authors greatly acknowledge partial financial supports of the Chair "Hydrology for resilient cities" endowed by Veolia, and of the Department of Science and Technology of the Brazilian Army. We would also like to thank Veolia for providing access to the hydrological model.

Declarations of Interest: The authors declare no conflict of interest. The funders had no role in the design of the study; in the collection, analyses, or

517 interpretation of data; in the writing of the manuscript, or in the decision to
518 publish the results.
519
520 **Credit Author Statement:** Igor Paz: Formal analysis, Investigation,
521 Methodology, Software, Validation, Visualization, Roles/Writing - original draft,
522 Writing - review & editing; Ioulia Tchiguirinskaia: Conceptualization, Formal
523 analysis, Funding acquisition, Investigation, Methodology, Project
524 administration, Resources, Supervision, Writing - review & editing; Daniel
525 Schertzer: Conceptualization, Formal analysis, Funding acquisition,
526 Investigation, Methodology, Project administration, Resources, Supervision,
527 Writing - review & editing.
528
529 **References**
530
531 Allegretti, M., Bertoldo, S., Prato, A., Lucianaz, C., Rorato, O., Notarpietro, R., Gabella,
532 M., 2012. X-Band Mini Radar for Observing and Monitoring Rainfall Events.
533 Atmospheric and Climate Sciences, 2, 290–297,
534 http://dx.doi.org/10.4236/acs.2012.23026.
535
536 Alves de Souza, B., da Silva Rocha Paz, I., Ichiba, A., Willinger, B., Gires, A., Amorim,
537 J.C.C., de Miranda Reis, M., Tisserand, B., Tchiguirinskaia, I., Schertzer, D., 2018.
538 Multi-hydro hydrological modelling of a complex peri-urban catchment with storage
539 basins comparing C-band and X-band radar rainfall data. Hydrological Sciences
540 Journal, 63 (11), 1619–1635, doi.org/10.1080/02626667.2018.1520390.
541

Arnone, E., Pumo, D., Francipane, A., La Loggia, G., Noto, L.V., 2018. The role of urban growth, climate change, and their interplay in altering runoff extremes. Hydrological Processes, 32, 1755-1770, https://doi.org/10.1002/hyp.13141.

Austin, P.M., 1987. Relationship between measured radar reflectivity and surface rainfall. Mon. Weather Rev., 115, 1053-1070, doi:10.1175/1520-0493(1987)115<1053:RBMRRA>2.0.CO;2.

Berne, A., Delrieu, G., Creutin, J.-D., Obled, C., 2004. Temporal and spatial resolution of rainfall measurements required for urban hydrology. J. Hydrol., 299 (3), 166–179, doi.org/10.1016/j.jhydrol.2004.08.002.

Bringi, V.N., Chandrasekar, V., 2001. Polarimetric Doppler Weather Radar: Principles and Applications, Cambridge, Cambridge University Press.

Chandrasekar, V., Baldini, L., Bharadwaj, N., Smith, P.L., 2015. Calibration procedures for global precipitation-measurement ground-validation radars. URSI Radio Science Bulletin, 88, 4, doi.org/10.23919/URSIRSB.2015.7909473.

de Lima, M.I.P., Grasman, J., 1999. Multifractal analysis of 15-min and daily rainfall from a semi-arid region in Portugal. J. Hydrol., 220 (1-2), 1–11, doi.org/10.1016/S0022-1694(99)00053-0.

Deidda, R., 2000. Rainfall downscaling in a space-time multifractal framework. Water Resour. Res., 36, 1779–1794, doi.org/10.1029/2000WR900038.

568 Einfalt, T., Arnbjerg-Nielsen, K., Golz, C., Jensen, N.-E., Quirmbach, M., Vaes, G.,
569 Vieux, B., 2004. Towards a roadmap for use of radar rainfall data in urban drainage. J.
570 Hydrol., 299, 186–202, doi:10.1016/j.jhydrol.2004.08.004.
571
572 Einfalt, T., Jessen, M., Mehlig, B., 2005. Comparison of radar and raingauge
573 measurements during heavy rainfall. Water Science & Technology, 51(2), 195-201,
574 https://doi.org/10.2166/wst.2005.0048.
575
576 Fabry, F., Bellon, A., Duncan, M.R., Austin, G.L., 1994. High resolution rainfall
577 measurements by radar for very small basins: the sampling problem reexamined. J.
578 Hydrol., 161 (1-4), 415–428, http://dx.doi.org/10.1016/0022-1694(94)90138-4.
579
580 Falconer, K., 1990. Fractal geometry: mathematical foundations and applications.
581
582 Feder, J., 1988. Fractals (physics of solids and liquids). Plennum, New York.
583
584 Fewtrell, T.J., Duncan, A., Sampson, C.C., Neal, J.C., Bates, P.D., 2011.
585 Benchmarking urban flood models of varying complexity and scale using high
586 resolution terrestrial LiDAR data. Phys. Chem. Earth, Parts A/B/C, 36 (7–8), 281–291,
587 doi.org/10.1016/j.pce.2010.12.011.
588
589 Figueras i Ventura, J., Boumahmoud, A.-A., Fradon, B., Dupuy, P., Tabary, P., 2012.
590 Long-term monitoring of French polarimetric radar data quality and evaluation of
591 several polarimetric quantitative precipitation estimators in ideal conditions for
592 operational implementation at C-band. Q. J. R. Meteorol. Soc., 138, 2212–2228,
593 doi:10.1002/qj.1934.
594

595 Furusho, C., Andrieu, H., Chancibault, K., 2014. Analysis of the hydrological behaviour
596 of an urbanizing basin. Hydrol. Process., 28, 1809–1819, doi: 10.1002/hyp.9706.
597
598 García-Marín, A.P., Jiménez-Hornero, F.J., Ayuso-Muñoz, J.L., 2008. Universal
599 multifractal description of an hourly rainfall time series from a location in southern
600 Spain. Atmósfera, 21(4), 347–55.
601
602 Gires, A., Abbes, J.-B., da Silva Rocha Paz, I., Tchiguirinskaia, I., Schertzer, D., 2018.
603 Multifractal characterisation of a simulated surface flow: a case study with Multi-Hydro
604 in Jouy-en-Josas, France. Journal of Hydrology, 558, 482–495,
605 https://doi.org/10.1016/j.jhydrol.2018.01.062.
606
607 Gires, A., Tchiguirinskaia, I., Schertzer, D., Ochoa-Rodriguez, S., Willems, P., Ichiba,
608 A., Wang, L.-P., Pina, R., Van Assel, J., Bruni, G., Tuyls, D.M., ten Veldhuis, M.-C.,
609 2017. Fractal analysis of urban catchments and their representation in semi-distributed
610 models: imperviousness and sewer system. Hydrol. Earth Syst. Sci., 21, 2361–2375,
611 doi:10.5194/hess-21-2361-2017.
612
613 Grassberger, P., 1983. Generalized dimensions of strange attractors. Physics Letters
614 A, 97(6) :227–230.
615
616 Hentschel, H., Procaccia, I., 1983. The infinite number of generalized dimensions of
617 fractals and strange attractors. Physica D: Nonlinear Phenomena, 8(3):435–444.
618
619 Hoang, C.T., 2011. Prise en compte des fluctuations spatio-temporelles pluies-débits
620 pour une meilleure gestion de la ressource en eau et une meilleure évaluation des
621 risques. Ph.D. thesis, Université Paris-Est, France.
622

623 Ichiba, A., 2016. X-band radar data and predictive management in urban hydrology.
624 Ph.D. thesis, Earth Sciences, Université Paris-Est, France.
625
626 Illingworth, A.J., Blackman, T.M., 2002. The need to represent raindrop size spectra as
627 normalized gamma distributions for the interpretation of polarization radar
628 observations. Journal of Applied Meteorology, 41 (3), 286–297,
629 https://doi.org/10.1175/1520-0450(2002)041<0286:TNTRRS>2.0.CO;2.
630
631 Ladoy, P., Schmitt, F., Schertzer, D., Lovejoy, S., 1993. Variabilité temporelle
632 multifractale des observations pluviométriques à Nîmes. C. R. Acad. Sci. II, 317, 775–
633 782.
634
635 Lavallée, D., Lovejoy, S., Schertzer, D., Ladoy, P., 1993. Nonlinear variability and
636 landscape topography: analysis and simulation. Fractals in geography, pp. 158–192.
637
638 Lo Conti, F., Francipane, A., Pumo, D., Noto, L. V., 2015. Exploring single polarization
639 X-band weather radar potentials for local meteorological and hydrological applications.
640 Journal of Hydrology, 531, 508–522, https://doi.org/10.1016/j.jhydrol.2015.10.071.
641
642 Lovejoy, S., Schertzer, D., Tsonis, A., 1987. Functional box-counting and multiple
643 elliptical dimensions in rain. Science, 235(4792):1036–1038.
644
645 Mandelbrot, B.B. 1967. How long is the coast of Britain. Science, 156(3775):636–638.
646
647 Mandelbrot, B.B., 1974. Intermittent turbulence in self-similar cascades: divergence of
648 high moments and dimension of the carrier. Journal of Fluid Mechanics, 62(2):331–
649 358.
650

651 Mandelbrot, B.B., 1977. Fractals: form, chance and dimension.
652
653 Mandelbrot, B.B., Pignoni, R., 1983. The fractal geometry of nature.
654
655 Marshall, J.S., Palmer, W.M.K, 1948. The distribution of raindrops with size. Journal of
656 Meteorology, 5, 165–166.
657
658 National Research Council of the National Academies. Urban Meteorology:
659 Forecasting, Monitoring, and Meeting Users' Need; National Academy Press:
660 Washington, WA, USA, 2012.
661
662 Ochoa-Rodriguez, S., Wang , L.-P., Gires, A., Pina, R., Reinoso-Rondinel, R., Bruni,
663 G., Ichiba, A., Gaitan, S., Cristiano, E., van Assel, J., Kroll, S., Murlà-Tuyls, D.,
664 Tisserand, B., Schertzer, D., Tchiguirinskaia, I., Onof, C., Willems, P., ten Veldhuis, M.-
665 C., 2015. Impact of spatial and temporal resolution of rainfall inputs on urban
666 hydrodynamic modelling outputs: A multi-catchment investigation. J. Hydrol., 531, 389–
667 407, doi.org/10.1016/j.jhydrol.2015.05.035.
668
669 Olsson, J., Niemczynowicz, J., 1996. Multifractal analysis of daily spatial rainfall
670 distributions. J. Hydrol., 187, 29–43, doi.org/10.1016/S0022-1694(96)03085-5.
671
672 Parisi, G. and Frisch, U., 1985. A multifractal model of intermittency. Turbulence and
673 predictability in geophysical fluid dynamics and climate dynamics, pp. 84–88.
674
675 Paz, I.S.R., 2018. Quantifying the rain heterogeneity by X-band radar measurements
676 for improving flood forecasting. Ph.D. thesis, Université Paris-Est, France.
677

678 Paz, I., Willinger, B., Gires, A., Ichiba, A., Monier, L., Zobrist, C., Tisserand, B.,
679 Tchiguirinskaia, I., Schertzer, D., 2018. Multifractal Comparison of Reflectivity and
680 Polarimetric Rainfall Data from C-and X-Band Radars and Respective Hydrological
681 Responses of a Complex Catchment Model. Water, 10 (3), 269,
682 doi:10.3390/w10030269.
683
684 Paz, I., Willinger, B., Gires, A., Alves de Souza, B., Monier, L., Cardinal, H., Tisserand,
685 B., Tchiguirinskaia, I., Schertzer, D., 2019. Small-Scale Rainfall Variability Impacts
686 Analyzed by Fully-Distributed Model Using C-Band and X-Band Radar Data. Water, 11
687 (6), 1273, doi:10.3390/w11061273.
688
689 Peleg, N., Ben-Asher, M., Morin, E., 2013. Radar subpixel-scale rainfall variability and
690 uncertainty: lesson learned from observations of a dense rain-gauge network. Hydrol.
691 Earth Syst. Sci., 17, 2195-2208, doi:10.5194/hess-17-2195-2013.
692
693 Pina, R., Ochoa-Rodríguez, S., Simões, N., Mijic, A., Sa Marques, A., Maksimovič, C.,
694 2016. Semi-distributed or fully distributed rainfall-runoff models for urban pluvial flood
695 modelling? Water, 8 (2), 58, doi:10.3390/w8020058.
696
697 Pumo, D., Arnone, E., Francipane, A., Caracciolo, D., Noto, L.V., 2017. Potential
698 implications of climate change and urbanization on watershed hydrology. Journal of
699 Hydrology, 554, 80-99, http://dx.doi.org/10.1016/j.jhydrol.2017.09.002.
700
701 Schertzer, D. and Lovejoy, S., 1984. On the dimension of atmospheric motions.
702 Turbulence and Chaotic phenomena in Fluids, pp. 505–512.
703

704 Schertzer, D. and Lovejoy, S., 1987. Physical modeling and analysis of rain and clouds
705 by anisotropic scaling multiplicative processes. Journal of Geophysical Research:
706 Atmospheres, 92(D8):9693–9714.
707
708 Schertzer, D. and Lovejoy, S., 1991. Nonlinear variability in geophysics.
709
710 Schertzer, D. and Lovejoy, S., 1997. Universal multifractals do exist!: Comments on “a
711 statistical analysis of mesoscale rainfall as a random cascade”. Journal of Applied
712 Meteorology, 36(9):1296–1303.
713
714 Schertzer, D. and Lovejoy, S., 2011. Multifractals and predictability in geophysics:
715 chaos and multifractal insights. The State of the Planet: Frontiers and Challenges in
716 Geophysics, pp. 317–334.
717
718 Schilling, W., 1991. Rainfall data for urban hydrology: what do we need? Atmos. Res.,
719 27, 5–21, doi:10.1016/0169-8095(91)90003-F.
720
721 Seed, A., Austin, G.L., 1990. Variability of Summer Florida Rainfall and its Significance
722 for the Estimation of Rainfall by Gages, Radar, and Satellite. Journal of Geophysical
723 Reseacrch, 90, D3, 2207-2215, https://doi.org/10.1029/JD095iD03p02207.
724
725 Segond, M.L., Neokleous, N., Makropoulos, C., Onof, C., Maksimović, Č., 2007.
726 Simulation and spatio-temporal disaggregation of multi-site rainfall data for urban
727 drainage applications. Hydrol. Sci. J. – J. Des Sci. Hydrol., 52 (5), 917–935,
728 http://dx.doi.org/10.1623/hysj.52.5.917.
729
730 Selex, 2015. Selex METEOR Manual. Selex: Rome, Italy.
731

732 Serinaldi, F., 2010. Multifractality, imperfect scaling and hydrological properties of
733 rainfall time series simulated by continuous universal multifractal and discrete random
734 cascade models. Nonlin. Processes Geophys., 17, 697–714, doi:10.5194/npg-17-697-
735 2010.
736
737 Soft, M., 2010. Infoworks CS 11.0 help file. Wallingford, UK.
738
739 Tessier, Y., Lovejoy, S., Schertzer, D., 1993. Universal multifractals in rain and clouds:
740 Theory and observations. J. Appl. Meteorol., 32 (2), 223–250,
741 https://doi.org/10.1175/1520- 0450(1993)032<0223:UMTAOF>2.0.CO;2.
742
743 Thorndahl, S., Einfalt, T., Willems, P., Nielsen, J.E., ten Veldhuis, M.-C., Arnbjerg-
744 Nielsen, K., Rasmussen, M.R., Molnar, P., 2017. Weather radar rainfall data in urban
745 hydrology. Hydrol. Earth Syst. Sci., 21, 1359–1380, doi:10.5194/hess-21-1359-2017.
746
747 Veneziano, D., Langousis, A., Furcolo, P., 2006 Multifractality and rainfall extremes: A
748 review. Water Resour. Res., 42, W06D15, doi:10.1029/2005WR004716.
749
750 Vieux, B.E., Vieux, J.E., 2005. Statistical evaluation of a radar rainfall system for sewer
751 system management. Atmospheric Research, 77, 1-4, 322-336,
752 https://doi.org/10.1016/j.atmosres.2004.10.032.
753
754 Villarini, G., Mandapaka, P. V., Krrajewski, W. F., Moore, R. J., 2008. Rainfall and
755 sampling uncertainties: A rain gauge perspective. J. Geophys. Res. Atmos., 113,
756 D11102, doi:10.1029/2007JD009214.
757

758 WMO, 2014. Guide to meteorological instruments and methods of observation. WMO-
759 No. 8. Available online: http://www.wmo.int/pages/prog/www/IMOP/CIMO-Guide.html
760 (Accessed on 14 July 2018).
761